MAGNETIC RESONANCE CORE ANALYSIS AT 0.3 T

Jonathan Mitchell
Schlumberger Gould Research, High Cross, Madingley Road, Cambridge CB3 0EL, UK

This paper was prepared for presentation at the International Symposium of the Society of Core Analysts held in Avignon, France, 8-11 September, 2014

ABSTRACT

Nuclear magnetic resonance (NMR) provides a powerful toolbox for laboratory-scale petrophysical characterization of reservoir core plugs. In recent years, considerable interest has been paid to low-field magnet technology. A resonance frequency of 2 MHz (field strength 0.05 T) is considered the industry standard for both well-log calibration and to provide quantitative measurements of porosity and saturation by minimising the influence of magnetic-susceptibility-induced "internal gradients," particularly in sandstones. However, the inherently poor signal-to-noise ratio (SNR) associated with such instruments limits the application of advanced techniques. Now there is renewed interest in employing three-dimensional (3D) magnetic resonance imaging (MRI) to monitor displacement processes in oil recovery studies. Previously, high-field medical MRI scanners were used for core analysis, but these studies suffered from a lack of quantification (saturation state) because of the presence of strong internal gradients. A field strength of 0.3 T (12.9 MHz for ^{1}H) offers the best of both worlds: quantitative saturation and fast imaging at millimetre resolution. This field strength also offers opportunities for heteronuclear detection. Sodium profiles are used to monitor displacement in high-salinity formations, and fluorine NMR can provide robust oil-brine contrast in model core-flood experiments. Measurements at intermediate field complement standard low field NMR core analysis.

INTRODUCTION

NMR well logging tools provide information on the porosity, permeability, and fluid saturation of a reservoir within the vicinity of the well bore [1]. The archetypal NMR well-logging measurement is a distribution of transverse T_2 relaxation time obtained using the Carr Purcell Meiboom Gill (CPMG) pulse sequence [2,3]. T_2 is considered an indication of the pore size (when a single fluid is present in the pores), or is used to distinguish fluid phases (oil, brine, gas). The integral area under the T_2 distribution is proportional to the total porosity and the moments of the distribution can be related to properties of the formation such as permeability [4]. Robust fluid phase discrimination is achieved through measurements of longitudinal T_1 relaxation time or molecular self-diffusion coefficient D correlated against T_2 in two-dimensional (2D) experiments [5,6]. Low magnetic fields are available down hole due to the technical challenges of generating a stronger field using a well logging tool.

Log calibration studies are performed in the laboratory on fluid-saturated core plugs. The industry standard for NMR core analysis is a ^{1}H resonance frequency of ν_0 = 2 MHz, corresponding to a magnetic field strength of B_0 = 0.05 T. The use of a low field magnet has the advantage of limiting pore-scale magnetic field distortions (so-called "internal gradients") caused by the solid/fluid susceptibility contrast [7]. It is the magnetic field dependence of internal gradients that necessitates similar frequencies for laboratory instruments and logging tools: if laboratory data are to be used for log calibration, the measurements must be based on common measurement physics.

There is a significant challenge associated with laboratory measurements at 2 MHz, namely the inherently poor SNR. Despite recent improvements in radio frequency (rf) probe design, monitoring flow through porous media or detecting very short relaxation time components in shales remains challenging, while multi-dimensional imaging is impractical. Therefore, low-field NMR core analysis can be complemented with measurements at a higher magnetic field strength to provide additional information on fluid distribution and transport in porous rocks. Here, the capabilities of a commercial intermediate-field NMR spectrometer, designed as an imaging platform, are demonstrated. For favorable rock formations like carbonates (low magnetic susceptibility contrast), quantitative measurements of porosity and saturation are obtained. When interpretation of T_2 relaxation times becomes unreliable due to the presence of internal gradients, quantitative porosity and saturation values are obtained instead using T_1 relaxation time analysis. At B_0 = 0.3 T, sufficient SNR is available to obtain 2D or 3D images with millimeter resolution in just a few minutes. Macroscopic heterogeneities such as fossils, non-porous mineral deposits, and dissolution vugs, or non-uniform saturation, are observable at this resolution. Furthermore, the use of an intermediate-field magnet enables heteronuclear detection, such as measurements of sodium in an aqueous salt solution where the ^{23}Na resonance frequency is ν_0 = 3.4 MHz. The sodium nucleus provides unambiguous detection of brine in multiphase core flood experiments [8].

HARDWARE

The intermediate-field spectrometer used in this study is an Oxford Instruments bench-top "Rock Core Analyzer." The NMR system comprises a vertical bore B_0 = 0.3 T permanent magnet thermostated to 35^{o}C. The B_0 field (z-axis) is horizontal in the bench-top configuration, allowing the use of a solenoid rf resonator that generates a B_1 field along the vertical y-axis; see **Figure 1**. The cylindrical rf probe has dimensions of 60 mm × 51 mm (length × diameter). The rf pulses are supplied by a 1 kW LPPA 13010 linear pulse power amplifier {Dressler HF-Technik, Germany} with the input attenuated to provide a maximum output of 500 W. Typical 90^{o} and 180^{o} rf pulse durations are t_{90} = 15 µs and t_{180} = 30 µs, respectively. The physical recovery time (dead time) of the rf system is approximately t_{dead} = 20 µs at 12.9 MHz, permitting a minimum CPMG echo time of t_e = 70 µs. Magnetic field gradients up to G_{max} = 0.25 T m^{-1} (x and y) or G_{max} = 0.45 T m^{-1} (z) were provided by slab format gradient coils, driven by three high performance ERA

9180B amplifiers {ERA 5, Somerset, UK}. The stronger gradient on the z axis is available for diffusion measurements. The linear region of the applied field gradient along the y-axis corresponds to the central 50 mm of the rf probe, which defines the maximum sample length. The gradient plates are cooled to 20°C using a ThermoFlex 1400 water chiller {Thermo Fisher Scientific, Waltham MA, USA}. Field homogeneity to better than $\Delta B_0 = 1.5 \times 10^{-2}$ mT is achieved over the maximum cylindrical sample volume of 50 mm × 48 mm (length × diameter) that can be reasonably accommodated. The electric shim coils were driven by an Oxford Instruments DSP-20 shim controller. An Oxford Instruments Maran DRX-HF spectrometer was used for pulse sequence generation and data acquisition. For ^{23}Na detection, a spare rf resonator was converted to an active damping probe with feedback pre-amplifier {MRF Innovations, UK} to minimize the dead time of the receiver and maximize the SNR.

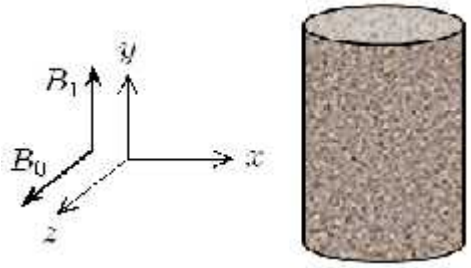

Figure 1. Typical orientation of a core-plug in a permanent magnet. The magnetic field B_0 is aligned along the z-axis by convention; the rf B_1 field is applied along the y-axis.

CONVENTIONAL CORE ANALYSIS

For log calibration, a 2 MHz spectrometer is still recommended. However, to explore the capabilities and limitations of higher field instruments, standard analysis methods are applied here to a suite of rock plugs at 12.9 MHz.

Samples. A suite of eight rocks spanning a range of porosities and permeabilities was studied to assess the degree of quantification available at B_0 = 0.3 T. Petrophysical properties of the cored plugs are given in **Table 1**. The cylindrical plugs (diameter of 38 mm) were extracted from blocks of quarried material and trimmed to length (50 mm) prior to drying for 24 h at 90°C in a vacuum oven. Helium porosity and nitrogen permeability were determined on the dry samples. The plugs were then vacuum saturated with low-salinity brine. The core plugs were weighed dry and wet (before and after NMR measurement) to provide a gravimetric determination of the brine content. No drainage (liquid loss) was observed during the NMR measurement interval.

NMR experiments. Transverse T_2 relaxation times were determined using the CPMG experiment [2,3]. The temporal separation of spin echoes was t_e = 100 μs. A total of 11 data points were acquired at the top of each spin echo with a dwell time of t_{dw} = 1 μs. The duration of each CPMG sequence was 5 s, and 50,000 echoes were recorded. A recycle delay of t_{RD} = 10 s was included between each scan, and four repeat scans were summed to accommodate a quadrature phase cycle. Each complete CPMG acquisition lasted 60 s. Longitudinal T_1 relaxation times were determined using the rapid double-shot saturation-decay experiment [9,10]. A small tip angle excitation of $\alpha = 4^o$ was used with a fixed

inter-pulse spacing of τ_1 = 30 ms and an initial 90°-α delay of t_{spoil} = 2 ms. A total of n = 256 α pulses were applied. After each α pulse, a complete free induction decay (FID) was acquired comprising m = 1024 data points with a dwell time t_{dw} = 10 µs. A recycle delay of t_{RD} = 1 s was included between scans, and four repeat scans were summed to improve SNR and accommodate a quadrature phase cycle. Each T_1 decay was acquired in 68 s.

Table 1. Petrophysical Properties of Core Plugs

Rock	Lithology	Porosity / p.u.	Permeability / mD	T_1 porosity / p.u.	T_2 porosity / p.u.
Bentheimer	Sandstone	23	3503	22.9	24.1
Berea	Sandstone	25	1532	25.3	23.9
Birchover	Sandstone	14	40	13.6	14.9
Scioto	Sandstone	18	0.55	18.2	17.0
Portland	Limestone	21	760	21.2	21.2
Estaillades	Limestone	30	109	30.6	30.9
Doulting	Limestone	20	101	18.6	18.6
Stevns Klint	Chalk	51	7	50.1	50.1

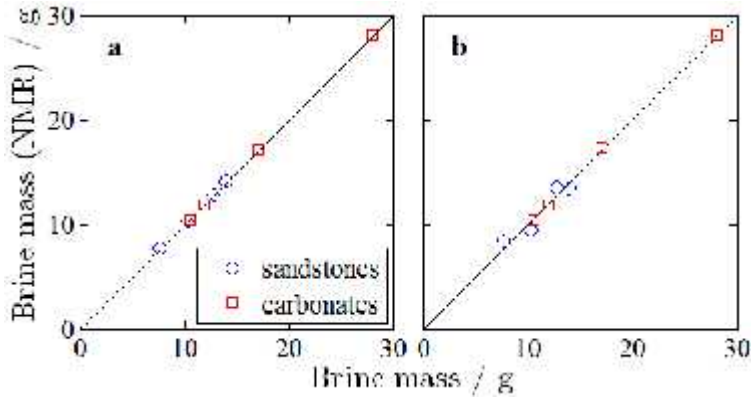

Figure 2. Comparison of brine mass determined gravimetrically and by total NMR signal from (a) T_1 and (b) T_2 data. The solid lines indicate equality between the measurement methods. The legend applies to both plots. Error bars on the gravimetric masses are consistent with the symbol size.

Porosity. A common petrophysical measurement using NMR is the determination of total porosity in a brine-saturated core plug. In order to compare signal amplitudes from a rock and a bulk (calibrated) liquid volume, it is necessary to remove any relaxation weighting. Quantitative signal intensity is readily obtained by integrating the area under a relaxation time distribution (T_1 or T_2). The total signal amplitudes obtained from T_1 and T_2 measurements were scaled according to the calibration mass. In the case of the T_1 measurement, **Figure 2**(a), the NMR data scale to match the mass of brine determined gravimetrically for all core plugs. For the T_2 measurement, **Figure 2**(b), the NMR data from the carbonates scale to match the gravimetic brine mass. However, the sandstone data are not consistent due to the presence of internal gradients that distort the NMR measurement and result in the generation of unphysical components in the T_2 distribution. For the sandstones, the error on the NMR estimate of brine mass from T_2 (±1 g) is significant when compared with the error in the T_1-derived mass (±0.1 g), as T_1 is known to be insensitive to internal gradients [11].

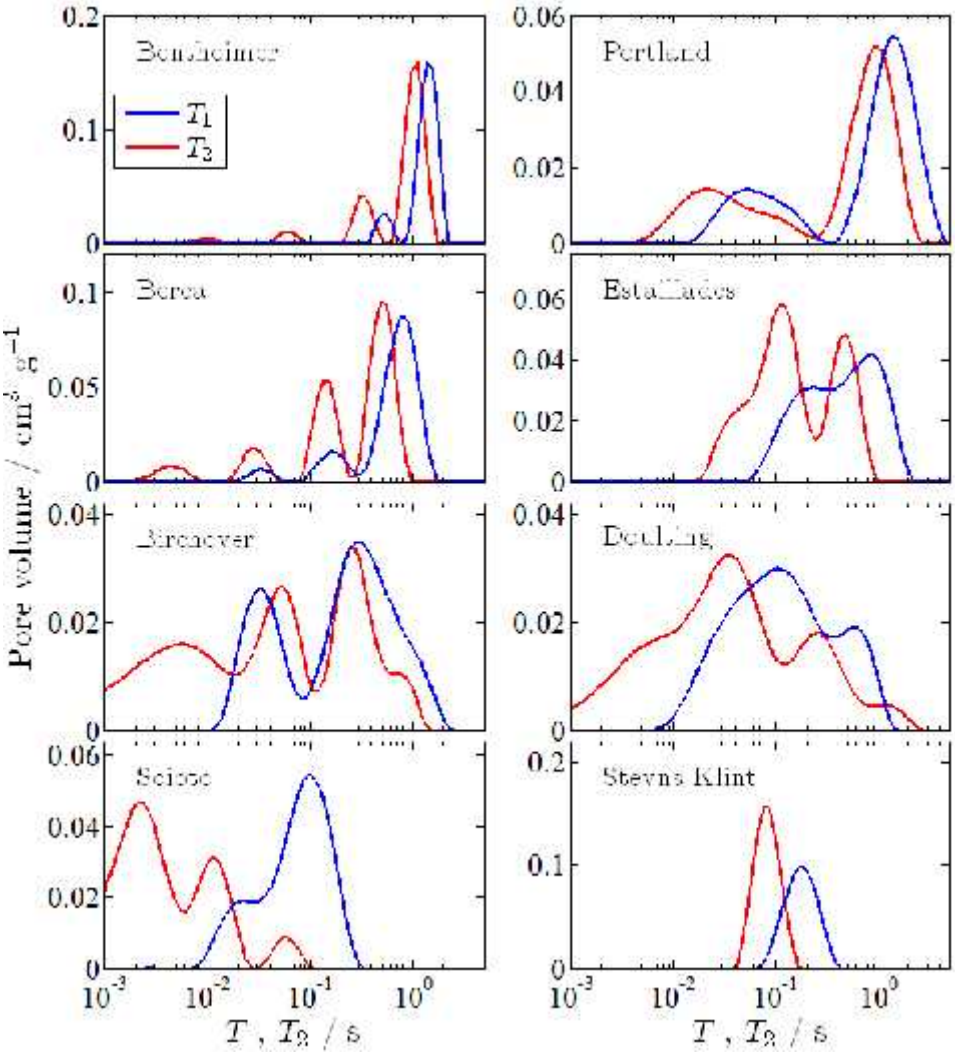

Figure 3. Relaxation time distributions of brine-saturated sandstone (left) and limestone (right) plugs. The legend applies to all plots. The distributions were generated using the method of Wilson [12].

Pore size distributions. Distributions of relaxation time are considered equivalent to pore body size distributions. The T_1 and T_2 relaxation time distributions for the suite of core plugs are shown in **Figure 3**. The T_1 data are expected to be an accurate reflection of the pore body size distributions, whereas the T_2 data are influenced by diffusion through the internal gradients in the sandstones. The T_1 distributions (solid blue lines) for Bentheimer and Berea are predominantly monomodal, with low-intensity components at shorter relaxation times attributed to water molecules bound to clays known to be present in these samples from thin section analysis. In previous work it has been argued that these components should not be interpreted as part of the pore size distribution, but are required when determining a total liquid signal [10]. Interpretation may be improved with a lithology-dependent surface relaxation model, although this approach increases the complexity of the analysis [13]. The Birchover T_1 distribution in **Figure 3** is bimodal,

suggesting the presence of a wide range of pore sizes in this heterogeneous formation. The Scioto T_1 distribution is also broad, although all the pores are small, leading to short relaxation times. The T_1 distributions of the limestones tend to be bimodal (Portland, Estaillades, and Doulting) where the short-time components correspond to microporosity (matrix pores) with pore diameters $d < 10$ μm and the long-time components correspond to macroporosity (e.g., dissolution vugs) with $d > 10$ μm. Stevns Klint is a homogeneous, microporous chalk (mudstone) and has a narrow, monomodal pore size distribution with a characteristic pore diameter of $d \approx 2$ μm.

For all the rocks represented in **Figure 3**, the T_2 relaxation times are shorter than T_1 such that the ratio $T_1/T_2 > 1$, as expected [11]. For the sandstones, additional T_2 components are seen at shorter relaxation times that do not correspond with components in T_1. These discrepancies are attributed to the influence of internal gradients on the T_2 measurement. The appearance of multiple relaxation time peaks in a T_2 distribution is a reliable indicator of internal gradients in rocks where the pore size distribution is expected to be smooth and (in the case of high-permeability sandstones) monomodal [7]. In the carbonate samples, the T_1 and T_2 distributions are qualitatively similar and the integral areas under the distributions provide quantitative measures of total porosity.

IMAGING

Bulk measurements of fluid properties in a core are important for well log calibration. However, the ability to spatially resolve information on liquid distribution has significant potential [14]. For example, visualization of macroscopic heterogeneity enables the selection of consistent plugs for measurement by conventional core analysis techniques, an important consideration when acquiring input parameters for simulation. To demonstrate the capabilities of bench-top MRI, 2D images of core plugs were acquired using the rapid acquisition with relaxation enhancement (RARE) pulse sequence [15]. The data are acquired in *k*-space (Fourier reciprocal of image space) are Fourier transformed to recover the image [16]. Example 2D images are shown in **Figure 4** for brine-saturated Bentheimer sandstone and Portland limestone. The homogeneous structure of the Bentheimer sandstone is obvious in these images, and no significant macroscopic variations are seen. In contrast, significant structures are observed in the heterogeneous Portland limestone. The high-intensity pixels (white) are associated with dissolution vugs (large pores), and the low-intensity pixels (black) are associated with fossils embedded in the formation. The long $T_{1,2}$ relaxation times of brine in these rocks makes them ideal for RARE imaging. Samples with shorter relaxation times can be imaged using pure-phase encoding techniques [17]. RARE images of porous materials are not typically considered quantitative unless steps are taken to compensate for relaxation [18]. Histograms of pore volume, derived from the RARE images in **Figure 4**, are shown in **Figure 5**. It is interesting to note that the mean porosities of $\phi = 0.241$ (Bentheimer) and $\phi = 0.214$ (Portland) determined from these histograms correspond well with the plug porosities in **Table 1**, suggesting that these RARE images are quantitative under the favourable circumstances.

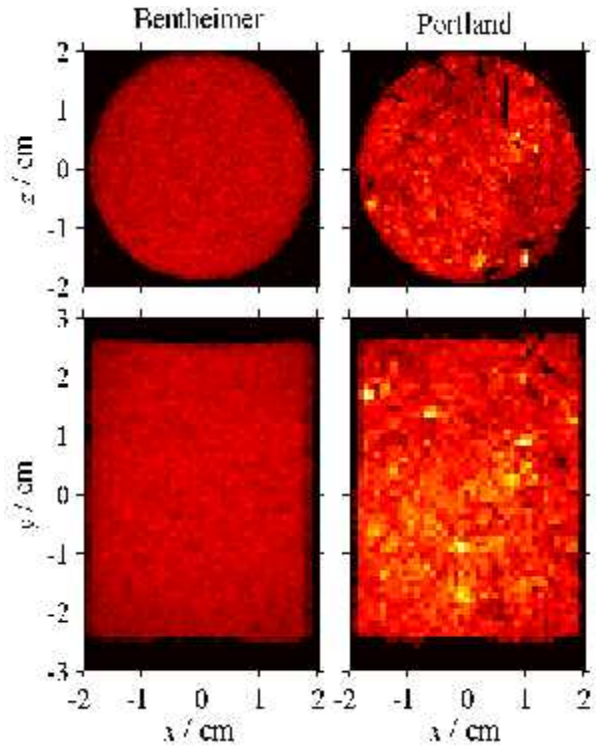

Figure 4. 2D RARE images obtained from brine-saturated Bentheimer (left) sandstone and Portland (right) limestone. The colour-scale indicates local porosity and ranges from black (no liquid) to white (no solid). The image slice is positioned in the centre of each plug. Distortions in the plug shape arise from a combination of imperfect alignment of the plug within the probe, B_0 and B_1 inhomogeneity, and magnetic susceptibility contrast which limits the maximum achievable image resolution. The *x*-*z* images were acquired with a pixel resolution of 782 µm × 782 µm with a 2 mm thick slice in *y*. The *x*-*y* images were acquired with a pixel resolution of 782 µm × 938 µm with a 2 mm thick slice in *z*. A RARE factor (number of echoes) of 64 was used, allowing the entire *k*-space raster to be sampled in a single scan; 128 repeat scans were acquired to improve the SNR. A recycle delay of t_{RD} = 6 s was used between scans, so the total time to acquire each 2D image was 20 min.

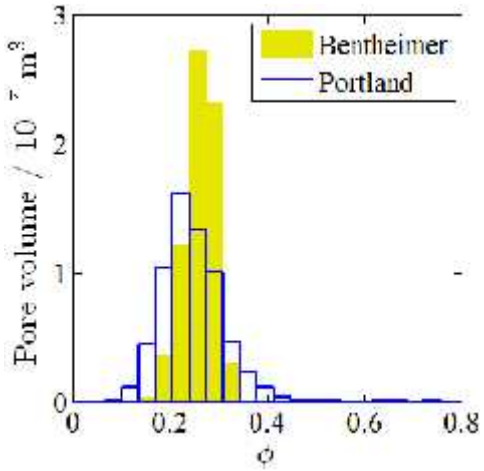

Figure 5. Porosity histograms obtained from the 2D RARE images in **Figure 4** for Bentheimer (yellow bars) sandstone and Portland limestone (blue/white bars). The intensity of each pixel was compared to the signal from a bulk water phantom to assign local porosity values. The pore volume scaling was based on the local porosity estimate, the volume of a pixel (1.47×10^{-9} m^3), and the pixel count for the given porosity.

Imaging of local saturation is a powerful method of monitoring oil recovery. Here, 3D images of an oil-saturated Bentheimer plug before and after brine injection are shown in **Figure 6**. The oil was a viscosity standard {S20; Poulten Selfe and Lee, Essex, UK} with η = 100 mPa s at 30°C. Initially, the oil saturation is uniform throughout the plug. After brine flooding, disconnected oil ganglia are distributed through the plug. This saturation state is attributed to pore-scale fingering due to the adverse mobility ratio between the high-viscosity oil and low-viscosity brine. In this particular example, there is no evidence of capillary end effects in the water-wet sandstone, as expected. Elsewhere, MRI has been used to visualize non-uniform oil saturation [19].

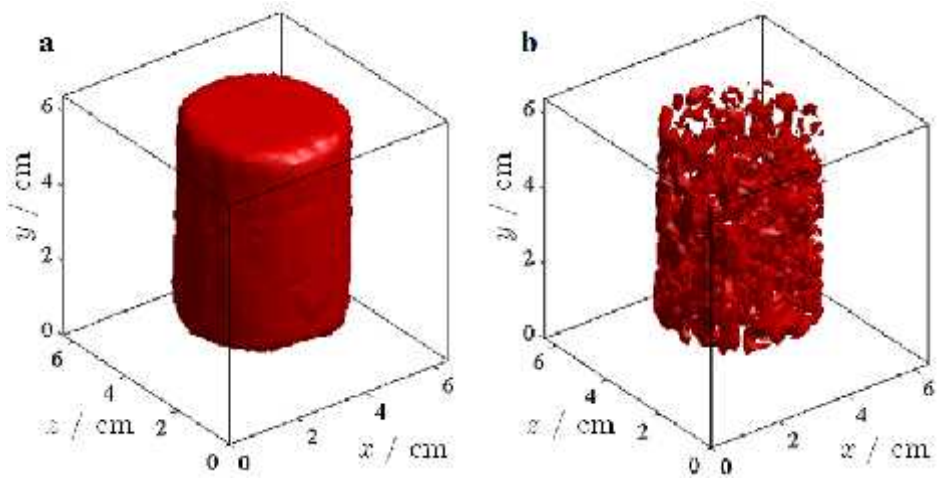

Figure 6. 3D RARE images of a Bentheimer sandstone plug (a) at initial oil saturation S_o = 0.93 and (b) post-brine flood at S_{or} = 0.23 remaining oil saturation (consistent with gravimetric effluent assay). Voxels containing predominately oil are shown. Voxels with an intensity corresponding to an oil saturation greater than S_o = 0.05 appear solid. Reasonable separation of the oil and brine signals was achieved by T_2 relaxation weighting (mean T_2 oil = 100 ms; mean T_2 brine = 1000 ms), although a low-intensity brine signal with T_2 < 100 ms is retained in the images. Brine was injected into the plug at increasing volumetric flow rates from 10^{-4} cm^3 s^{-1} to 7 cm^3 s^{-1} as part of a capillary desaturation measurement (to be published elsewhere). The images have an isotropic voxel resolution of 2 mm. A RARE factor of 32 was employed, allowing one phase raster (x) to be scanned during each acquisition. The other phase raster (z) was ramped over 32 successive experiments. A recycle delay of t_{RD} = 6 s was used between scans, and four repeat scans were summed, so the total time to acquire each 3D image was 15 min.

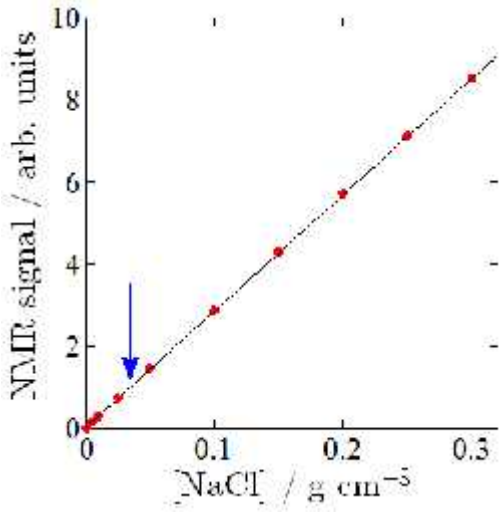

Figure 7. Correlation between NMR signal intensity and brine salinity over a wide range of sodium salt concentration. The sample volume was the same in each case. The error bars on the measurements are consistent with the marker size. At low salt concentrations, more scans were summed to improve the SNR (up to a maximum of 1024 scans at the lowest salt concentration of 0.005 g cm^{-3}). The solid line is a least-squares fit to the data. The average salinity of sea-water is [NaCl] = 0.035 g cm^{-3}, indicated by the arrow.

HETERONUCLEAR DETECTION

Many reservoirs contain sodium salts in brine, so detection of ^{23}Na is useful in petrophysics, enabling unambiguous detection of the aqueous phase [8]. Measurements of the ^{23}Na nucleus are 54 times less sensitive than for ^{1}H; nevertheless, detection of ^{23}Na at ν_0 = 3.4 MHz is feasible. The $T_1 \approx 40$ ms of sodium in solution permits a very short

recycle delay between scans, allowing repeat scans to be summed rapidly to improve the SNR. As salinity can vary widely between formations, it is important that the NMR signal amplitude remains proportional to the sodium content of the sample for quantitative analysis. **Figure 7** shows that the rf system on the 0.3 T magnet is insensitive to the salt concentration (electrical conductivity) from [NaCl] = 0 g cm^{-3} (freshwater) to 300 g cm^{-3} (almost salt-saturated brine at 20°C). When measuring ^{23}Na in low salinity brine at 0.3 T, the inherent poor SNR ensures that only one-dimensional (1D) profiles may be acquired in a reasonable experimental time. An example of salinity profiling is shown in **Figure 8**, where a variation in salt content of a brine-saturated glass bead pack has been monitored. On brine injection, **Figure 8**(a), the ^{23}Na front moves through the cell linearly with time. At the end of the flood, the profile shows a non-uniform salt distribution as a consequence of the sample cell geometry. The bead pack was left for 2 h, during which time salt diffusion resulted in a more uniform profile. A second flood was performed, where freshwater was injected into the brine-saturated bead pack; see **Figure 8**(b). The displacement of salt occurred via two separate processes as the low-density water flowed up through the high-density brine. Initially, salinity decreased over the entire cell. Then a reduction in the local salt content was observed moving from the outlet to the inlet face of the sample cell. Eventually a minimum salt content was reached, after which no further desalinization occurred. In this particular example, the liquid distribution was dominated by the cell geometry. Nevertheless, it is a clear demonstration of the feasibility of monitoring local salinity using a B_0 = 0.3 T magnet.

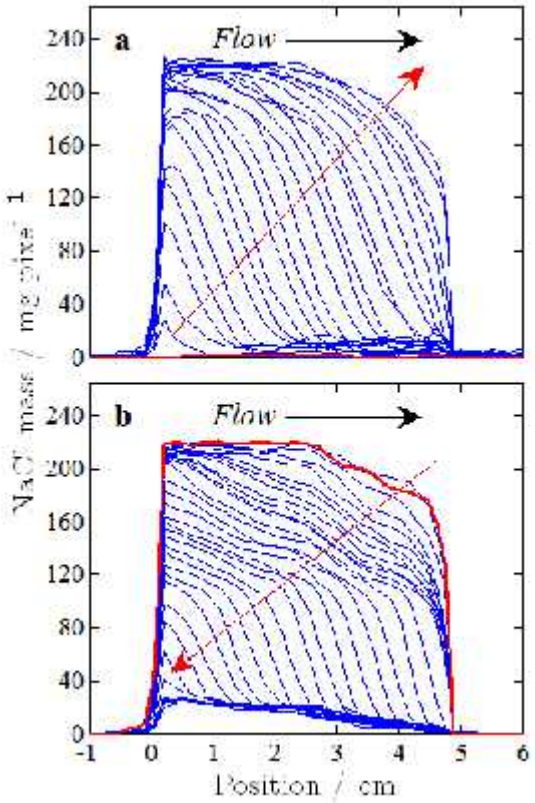

Figure 8. Sodium-salt profiles of (a) brine injection into a water saturated glass bead pack and (b) water injection into a brine saturated glass bead pack. The red arrows indicate increasing time; the first profile is highlighted in red in each case. The bead pack comprised non-porous borosilicate ballotini (nominal bead diameter of 100 μm) in a simple cylindrical Perspex flow cell with sample dimensions of 50 mm × 38 mm (length × diameter). The inlet and outlet ports opened directly into the bead pack without distribution platens to ensure non-uniform displacement for the purpose of this demonstration. The cell was mounted vertically in the magnet, with flow always from bottom to top (black arrows). The bead pack was initially saturated with freshwater, into which an [NaCl] = 0.3 g cm^{-3} brine was injected at a constant volumetric flow rate of 0.001 cm^3 s^{-1}. Profiles were acquired every 3 min during the flood. The signal amplitude was rescaled to local salt mass based on the calibration data in **Figure 7**.

Nuclei other than ^{1}H and ^{23}Na can be detected at B_0 = 0.3 T. Obvious candidates for use in petrophysics are ^{7}Li and ^{19}F [20]. An example is given in **Figure 9** where three immiscible phases are identified by heteronuclear detection. It is clear that careful selection of the nucleus can provide robust liquid phase discrimination in rock formations where ^{1}H detection alone would not adequately separate oil and brine.

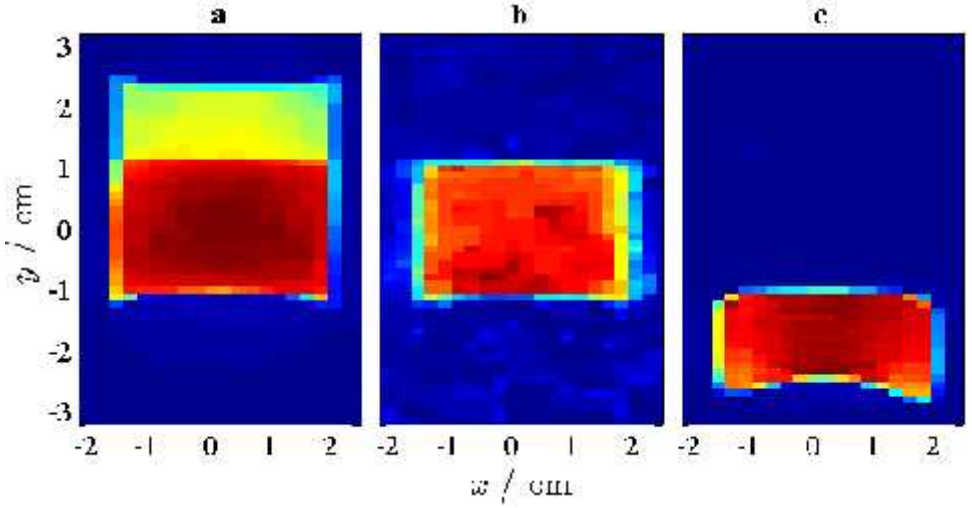

Figure 9. RARE images of a bulk liquid phantom containing (top to bottom) S20 oil, high-salinity brine, and perfluorinated oil {Fluorinert; 3M, St. Paul, MN, USA}. Images were acquired by detecting (a) ^{1}H, (b) ^{23}Na, and (c) ^{19}F. Each image had an acquisition time of 10 min, although the number of scans (determined by T_1) and slice thickness (determined by sensitivity of the nucleus) varied. The z slice thickness was (a) 5 mm, (b) 20 mm, and (c) 10 mm. Images were acquired with an isotropic x-y pixel resolution of 1 mm. The intensity variation between the liquid layers in (a) is due to the relaxation contrast between oil and brine. The shape of the sample bottle base is visible in (c).

CONCLUSION

An NMR system operating at ν_0 = 12.9 MHz (^{1}H) is appropriate for determining the porosity and pore size distributions in carbonate formations using T_2 relaxation time data. When studying sandstones and porous media where internal gradients are significant, it is important to use a T_1-based measurement to guarantee quantitative results, as longitudinal relaxation is known to be insensitive to diffusion in porous media [11]. Using an increased magnetic field strength enables rapid multidimensional imaging of liquid distribution in core plugs and reveals macroscopic structural heterogeneities. Saturation imaging is important for monitoring displacement processes during core floods, especially when capillary end effects dominate the distribution in short plugs [21]; these data can be compared directly to simulation results. The ability to access nuclei other than ^{1}H, notably ^{23}Na in brines, provides unambiguous discrimination of liquid phases. Further advantages not explored in this paper are also brought by the increased field strength. In particular, the very short rf probe recovery times are appropriate for studies of shales and other unconventional formations [22,23], and the SNR enables robust measurements of flow [24]. An intermediate-field imaging magnet provides a powerful and versatile complement to standard low-field NMR core analysis.

ACKNOWLEDGEMENTS

The author thanks Edmund Fordham for initiating the use of the intermediate-field magnet for core analysis. Laurence Hawkes and John Staniland assisted with the sample preparation. Thin section analysis was performed by Corex, Aberdeen, UK. Magnet shimming was performed by Ian Nicholson (MRF Innovations, UK).

REFERENCES

1. Kleinberg, R.L. "Well logging overview," *Concept. Magn. Reson.* (2001) **13**, 342-343.
2. Carr, H. and E. Purcell "Effects of diffusion on free precession in NMR experiments," *Phys. Rev.* (1954) **94**, 630-638.
3. Meiboom, S. and D. Gill "Modified spin-echo method for measuring nuclear relaxation times," *Rev. Sci. Instrum.* (1958) **29**, 668-691.
4. Borgia, G.C., R.J.S. Brown and P. Fantazzini "Different average nuclear magnetic resonance relaxation times for correlation with fluid-flow permeability and irreducible water saturation in water-saturated sandstones" *J. Appl. Phys.* (1997) **82**, 4197-4204.
5. Song, Y.Q., L. Venkataramanan, M.D. Hurlimann, M. Flaum, P. Frulla and C. Straley "T_1-T_2 correlation spectra obtained using a fast two-dimensional Laplace inversion," *J. Magn. Reson.* (2002) **154**, 261-268.
6. Hurlimann, M.D., L. Venkataramanan and C. Flaum "The diffusion-spin relaxation time distribution function as an experimental probe to characterize fluid mixtures in porous media," *J. Chem. Phys.* (2002) **117**, 10223-10232.
7. Mitchell J., T.C. Chandrasekera, M.L. Johns, L.F. Gladden and E.J. Fordham "Nuclear magnetic resonance relaxation and diffusion in the presence of internal gradients: The effect of magnetic field strength" *Phys. Rev. E* (2010) **81**, 026101.
8. Washburn, K.E. and G. Madelin "Imaging of multiphase fluid saturation within a porous material via sodium NMR," *J. Magn. Reson.* (2010) **202**, 122-126.
9. Chandrasekera, T.C., J. Mitchell, E.J. Fordham, L.F. Gladden and M.L. Johns "Rapid encoding of T_1 with spectral resolution in *n*-dimensional relaxation correlations," *J. Magn. Reson.* (2008) **194**, 156-161.
10. Mitchell J. "Rapid measurements of heterogeneity in sandstones using low-field nuclear magnetic resonance," *J. Magn. Reson.* (2014) **240**, 52-60.
11. Kleinberg, R.L., S.A. Farooqui and M.A. Horsfield "T_1/T_2 ratio and frequency dependence of NMR relaxation in porous sedimentary rocks," *J. Colloid Interf. Sci.* (1993) **158**, 195-198.
12. Wilson, J.D. "Statistical approach to the solution of 1st kind integral-equations arising in the study of materials and their properties," *J. Mater. Sci.* (1992) **27**, 3911-3924.
13. Quintero, L., A. Boyd, A. Gyllensten and F. El-Wazeer, "Comparison of permeability from NMR and production analysis in carbonate reservoirs," SPE paper 56798 presented at the Annual Technical Conference and Exhibition, Houston, Texas, USA, 3-6 October (1999).

14. Mitchell, J., T.C. Chandrasekera, D.J. Holland, L.F. Gladden and E.J. Fordham "Magnetic resonance imaging in laboratory petrophysical core analysis," *Phys. Rep.* (2013) **526**, 165-225.
15. Hennig, J., A. Nauerth and H. Freidburg "RARE imaging: a fast imaging method for clinical MR," *Magn. Reson. Med.* (1986) **3**, 823-833.
16. Callaghan, P.T. "Principles of Nuclear Magnetic Resonance Microscopy," Oxford University Press, Walton Street, Oxford OX2 6DP (1991).
17. Marica, F., Q. chen, A. Hamilton, C. Hall, T. Al and B.J. Balcom "Spatially resolved measurement of rock core porosity," *J. Magn. Reson.* (2006) **178**, 136-141.
18. Chen, Y.Y., L.P. Hughes, L.F. Gladden and M.D. Mantle "Quantitative ultra-fast MRI of HPMC swelling and dissolution," *J. Pharm. Sci.* (2010) **99**, 3462-3472.
19. Gharbi, R.B., N. Smaoui and E.J. Peters "Unstable EOR Displacements and Their Prediction Using the Karhunen-Loéve (K-L) Decomposition," SPE paper 39882 presented at the International Petroleum Conference and Exhibition, Vilkhannosa, Mexico, 3-5 March (1998).
20. Sarkar, S.N., J.J. Dechter and R. Komoroski "Multinuclear NMR imaging of fluid phases in Berea sandstone," *J. Magn. Reson. Ser. A* (1993) **102**, 314-317.
21. Mitchell, J., J. Staniland, A. Wilson, A. Howe, A. Clarke, E.J. Fordham, J. Edwards, R. Faber and R. Bouwmeester "Magnetic resonance imaging of chemical EOR in core to complement field pilot studies," SCA paper 30 presented at the International Symposium of the Society of Core Analysts, Aberdeen, Scotland, 27-30 August (2012).
22. Rylander, E., P.M. Singer, T. Jiang, R. Lewis, R. McLin and S. Sinclair "NMR T_2 distributions n the Eagle Ford shale: reflections on pore size," SPE paper 164554 presented at the Unconventional Resources Conference, The Woodlands, Texas, USA, 10-12 April (2013).
23. Fleury, M., S. Gautier, F. Norrant and E. Kohler "Characterization of nanoporous systems with low field NMR: application to kaolinite and smectite clays," SCA paper 23 presented at the International Symposium of the Society of Core Analysts, Austin, Texas, USA 18-21 September (2011).
24. Singer, P.M., G. Leu, E.J. Fordham and P.N. Sen "Low magnetic fields for flow propagators in permeable rocks," *J. Magn. Reson.* (2006) **183**, 167-177.